SCIENTIFIC REPORTS

OPEN

SUBJECT AREAS:
NANOSENSORS
SENSORS

Received
17 December 2013

Accepted
20 January 2014

Published
5 February 2014

Correspondence and requests for materials should be addressed to Z.L.J. (zljiang@mailbox.gxnu.edu.cn) or A.H.L. (ahliang2008@163.com)

Autocatalytic Oxidization of Nanosilver and Its Application to Spectral Analysis

Guiqing Wen, Yanghe Luo, Aihui Liang & Zhiliang Jiang

Key Laboratory of Ecology of Rare and Endangered Species and Environmental Protection of Ministry Education, Guangxi Normal University, Guilin 541004, China.

The stable yellow nanosilver (AgNP) and blue nanosilver (AgNPB) sols were prepared by the $NaBH_4$ procedure. The new nanocatalytic reaction of AgNP-NaCl-H_2O_2 was investigated by surface plasmon resonance (SPR) absorption, resonance Rayleigh scattering (RRS), surface-enhanced Raman scattering (SERS) and scanning electron microscope (SEM) techniques. The autocatalytic oxidization of Ag on AgNP surface by H_2O_2 was observed firstly and the AgNP/AgCl nanoparticles were characterized. The [Ag^+] from AgNP is different to the Ag^+ from $AgNO_3$ that adsorb on the AgNP surface. An autocatalytic oxidization mechanism was proposed to explain experimental phenomena. The relationship between the SPR absorption peaks and the RRS peaks of AgNPB was studied, and three characteristic RRS peaks called as out-of-plane quadrupole, out-of-plane dipole and in-plane dipole RRS peaks were observed firstly. Using AgNP as nanoprobe, a simple, sensitive and selective RRS method was developed for assay of H_2O_2 in the range of 2.0×10^{-8}-8.0×10^{-5} mol/L.

Nanoparticles have become research hot-spot in subjects such as physics, chemistry and materials due to their unique physical and chemical properties[1–5]. Based on the optical properties of nanoparticles, some new types of optical sensors and optoelectronic devices have been developed[6–9]. And the research of nanocatalysis and its application has become the important research directions in catalytic synthesis and nanoanalysis[10–16]. Among the nanocatalysis, the reports were mainly about nanogold catalysis and nano titanium dioxide photocatalysis[17–19]. Recently, some new nanocatalytic analytical methods were established[20–25], based on the catalysis of nanogold on the Cu(II)-glucose, $HAuCl_4$-ascrobic, $HAuCl_4$-citrate, Te(IV)-Sn(II), phosphomolybdic acid-formic acid and Ag(I)-hydroquinone particle reactions. It is rare report about nanosilver catalytic reaction. In synthesis of triangular nanosilver[26,27], the catalysis of nanosilver has been observed. Nanosilver modified by aptamer exhibited strong catalysis of the Cu_2O particle reaction of Fehling reagent-glucose, and it has been used to determine trace melamine by RRS technique[28]. Up to date, the autocatalytic oxidization of AgNP and its application in trace H_2O_2 analysis have not been reported.

The content of H_2O_2 is closely related to the photochemical reactions, oxidation-reduction reactions in natural water bodies. It is one of the important factors to affect the transfer, transformation, and ecological effect of chemical substances in water, and it is also one of the main reasons in the formation of acid rain[29]. In addition, the detection of H_2O_2 content is also very important in biochemical reactions, clinical test, food safety, and other fields[20–32]. At present, the spectral methods for H_2O_2 content are mainly including chemiluminescence, fluorescence, spectrophotometry, etc[33–35]. Among them, spectrophotometry is commonly used for its simple operation and low-cost. Recently, stabile metal nanoparticles, especially nanogold and nanosilver, are interesting to analyst. The spectral probe, based on nanogold color and RRS, have been used for determination of tumor markers, Hg^{2+}, H_2O_2, HCl and so on[36–41]. Compare to nanogold, AgNP has the advantage of low cost, and its aggregates do not interfere to the absorbance measurement since its absorption is very weak. In addition, stabile AgNP can be prepared by modern synthesis procedure and it has become novel spectral probe due to its strong SPR absorption, strong RRS and SERS effects of its aggregates[42]. It has been utilized to colorimetric chiral recognition of enantiomers, detection of DNA and melamine etc[28,43–45]. However, there is no report about the research and application of AgNP-NaCl-H_2O_2 autonanocatalytic system yet. In this paper, the reaction mechanism of AgNP-NaCl-H_2O_2 was studied by SPR, RRS[46–48], SERS and SEM techniques. Thus, two simple, rapid and sensitive spectral methods have been developed to determine H_2O_2.

Results

Scanning electron microscope. Stabile AgNP sol was prepared by $NaBH_4$ reduction of $AgNO_3$ in the presence of citrate. The SEM shows that they are spherical, with average size of 10 ± 2 nm (Fig. 1a). In AgNP-NaCl-H_2O_2

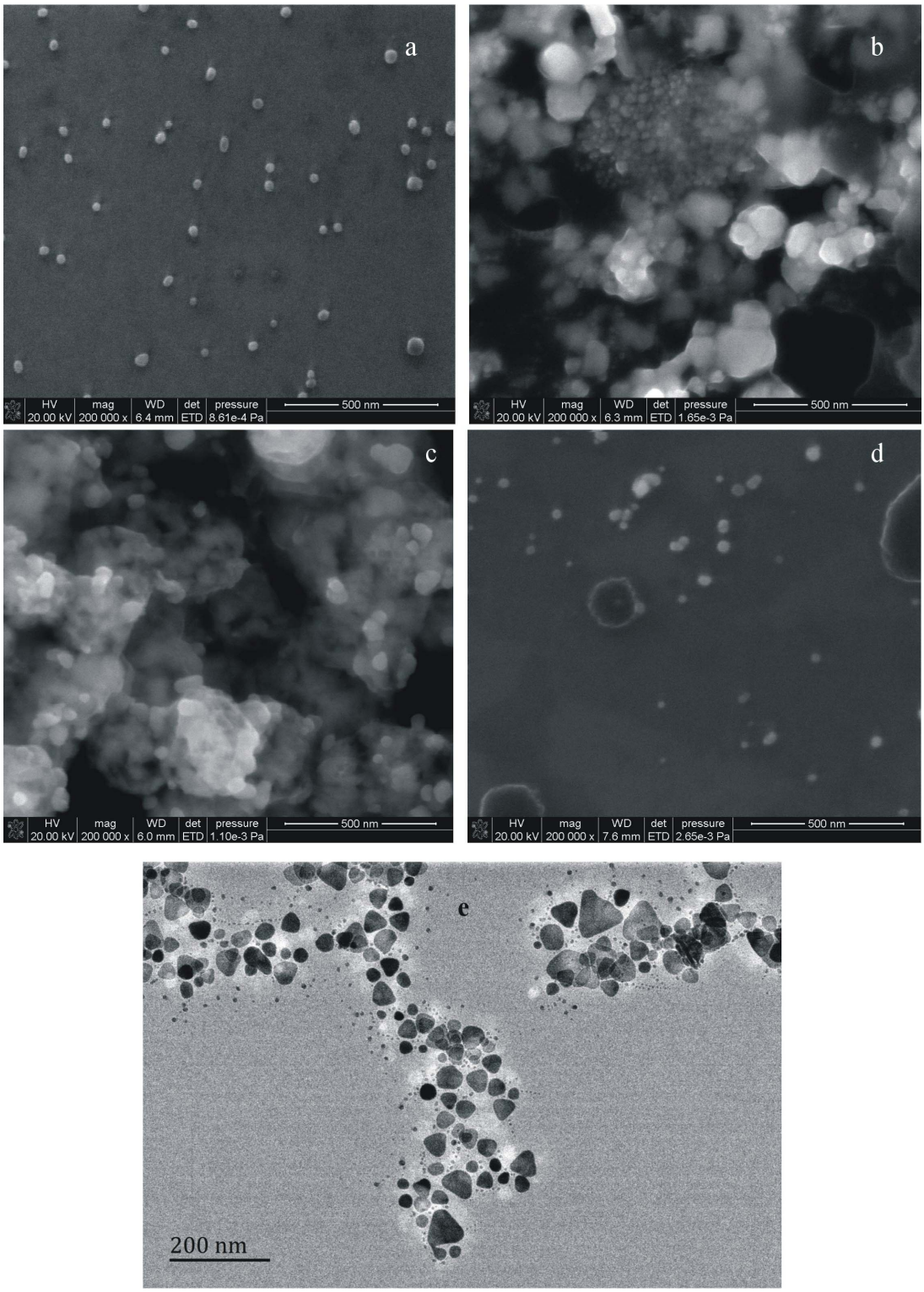

Figure 1 | SEM (a–d) and TEM (e) of AgNP. (a): 9.25×10^{-5} mol/L AgNP; (b):9.25×10^{-5} mol/L AgNP-2.0×10^{-3} mol/L NaCl-20×10^{-5} mol/L H_2O_2; (c): 9.25×10^{-5} mol/L AgNP-2.0×10^{-3} mol/L H_2SO_4-2.0×10^{-3} mol/L NaCl-3.75×10^{-5} mol/L $FeSO_4$-1.5×10^{-5} mol/L H_2O_2; (d): 5.0×10^{-5} mol/L AgNPB; (e): 5.0×10^{-5} mol/L AgNPB.

system, there is an autocatalytic oxidation reaction on the surface of AgNP to generate large Ag_n/AgCl particles with an average size of 60 ± 15 nm (Fig. 1b). In AgNP-H_2SO_4-NaCl-$FeSO_4$-H_2O_2 system, on one hand the autocatalytic oxidation reaction of AgNP generate Ag^+ on the surface, on the other hand surface atoms of AgNP also can generate Ag^+ by the Fenton oxidation reaction, so the large Ag_n/AgCl particles with an average size of 75 ± 16 nm was formed (Fig. 1c). SEM of AgNPB system shows that they are nearly spherical, with particle size between 6–100 nm and an average size of 40 ± 8 nm (Fig. 1d). The shape of AgNPB can not be observed satisfactorily by SEM, and the TEM of AgNPB system was done. Figure 2e indicated that there triangle nanosilver particles in the system, with the side length between 30–90 nm and an average side length of 45 ± 10 nm, in addition to the nearly spherical particles.

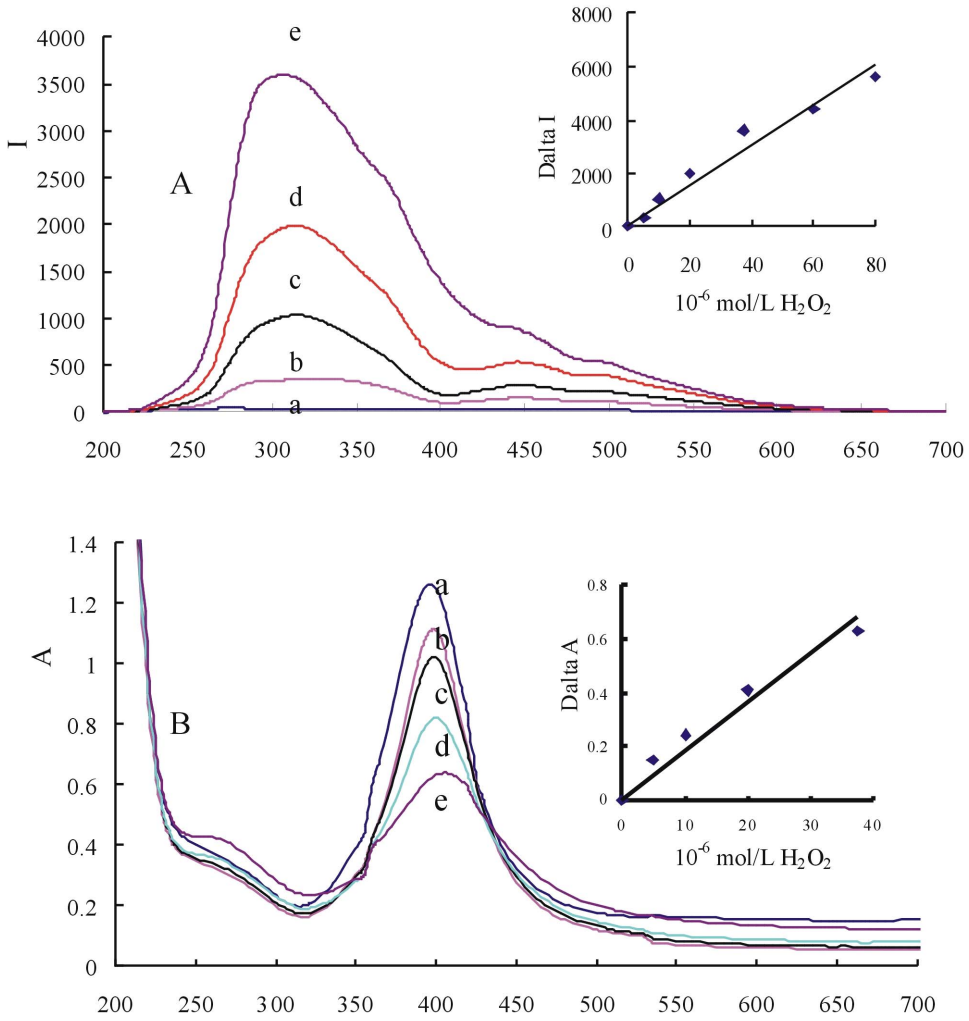

Figure 2 | RRS (A) and SPR (B) spectra of AgNP-NaCl-H_2O_2 system. (a): 9.25×10^{-5} mol/L AgNP -2.0×10^{-3} mol/L NaCl; (b):a-5.0×10^{-6} mol/L H_2O_2; (c): a-1.0×10^{-5} mol/L H_2O_2; (d): a-2.0×10^{-5} mol/L H_2O_2; (e): a-5.0×10^{-5} mol/L H_2O_2.

RRS spectra. In 2.0×10^{-3} mol/L NaCl medium, AgNPs are stabile and its RRS signal is very weak (Fig. 2A). With addition of H_2O_2, AgNP catalyze H_2O_2 to produce HO· and oxidize Ag atoms on the surface of AgNP to produce [Ag^+]. The [Ag^+] combined with Cl^- to form [AgCl] with strong hydrophobicity and then lead to form larger AgNP/AgCl aggregates that obviously enhanced the RRS intensity at 330 nm, 460 nm and 500 nm. The most sensitive RRS peak at 330 nm was selected to use in this paper. In existence of Fe(II) and H_2SO_4, the system had four RRS peaks at 290 nm, 360 nm, 455 nm and 500 nm (Fig. 1S). Fe(II) can hydrolyze and cause weak aggregation of AgNPs, and the blank increased. When adding H_2O_2, the Fenton reaction ($FeSO_4$-H_2O_2) also produced HO· that oxidize AgNP to form [Ag^+] and AgNP/[AgCl] particles. With H_2O_2 concentration increase its peak enhanced linearly due to more particles forming.

With addition of different concentration of $AgNO_3$ to the system of 2.0×10^{-3} mol/L NaCl-0.035% sodium citrate, AgCl particles were generated and exhibited strong scattering signal at 335 nm (Fig. 2S). The increased intensity $\Delta I_{335\ nm}$ was linear to $AgNO_3$ concentration in the range of 12.5–100×10^{-6} mol/L with the regression equation of $\Delta I_{335\ nm} = 53.3c_{Ag+} - 93$. For the system of 2.0×10^{-3} mol/L NaCl-0.035% sodium citrate-2.0×10^{-3} mol/L H_2SO_4-3.75×10^{-5} mol/L $FeSO_4$-$AgNO_3$, AgCl particles exhibited strong scattering signal at 335 nm (Fig. 3S). The increased intensity $\Delta I_{335\ nm}$ was linear to $AgNO_3$ concentration in the range of 12.5-100 $\times 10^{-6}$ mol/L with the regression equation of $\Delta I_{335\ nm} = 51.0c_{Ag+} +$ 116. This suggests that RRS signal's enhancement of AgNP-NaCl-H_2O_2 system is the result of the formation of AgCl particles. When adding different concentration of Ag^+ to the AgNP-NaCl-sodium citrate system, the RRS spectrum (Fig. 4S) is different with that of AgNP-NaCl-H_2O_2 and the former is weaker. It also suggests that [Ag^+] which produced by AgNP surface oxidation is different with that adsorption on the surface of the AgNP by adding $AgNO_3$. Compare to RRS spectra of NaCl-sodium citrate-$AgNO_3$ system, the RRS intensity of AgNP-NaCl-sodium citrate system is greatly reduced and has a valley at 395 nm, as the result of the strongest absorption of AgNPs at 395 nm.

SPR absorption spectra. Mie theory[49] pointed out that, spherical nanoparticles have only one SPR absorption peak. Spherical AgNP with diameter of 20–30 nm has the strongest SPR peak near 400 nm[50], which is out-of-plane dipole SPR absorption peak[51]. In the systems of NaCl and NaCl-H_2SO_4-$FeSO_4$, both have an AgNP SPR absorption peak at 395 nm (Fig. 2B, Fig. 5S). The absorbance at 395 nm of the two systems decreased linearly with the H_2O_2 concentration increased and can be chosen to determine H_2O_2. The $AgNO_3$-NaCl and $AgNO_3$-NaCl-H_2SO_4-$FeSO_4$ systems were examined by spectrophotometry. With addition of different $AgNO_3$ concentration to the two systems of 2.0×10^{-3} mol/L NaCl-0.035% sodium citrate and 2.0×10^{-3} mol/L NaCl-0.035% sodium citrate -2.0×10^{-3} mol/L H_2SO_4 -3.75×10^{-5} mol/L $FeSO_4$, the produced AgCl particles exhibited weak SPR peak at

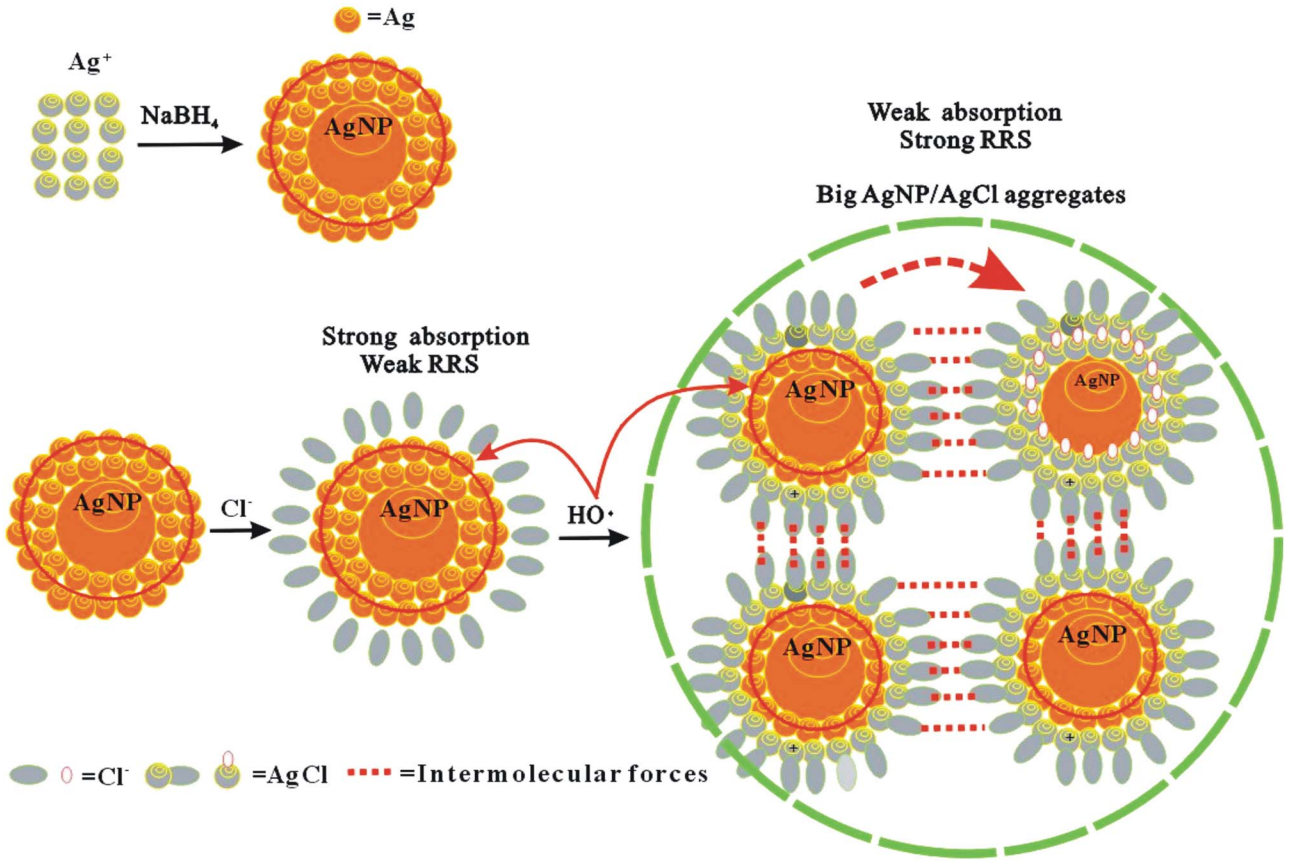

Figure 3 | **Principle of autocatalytic oxidization of AgNP to detect H_2O_2.**

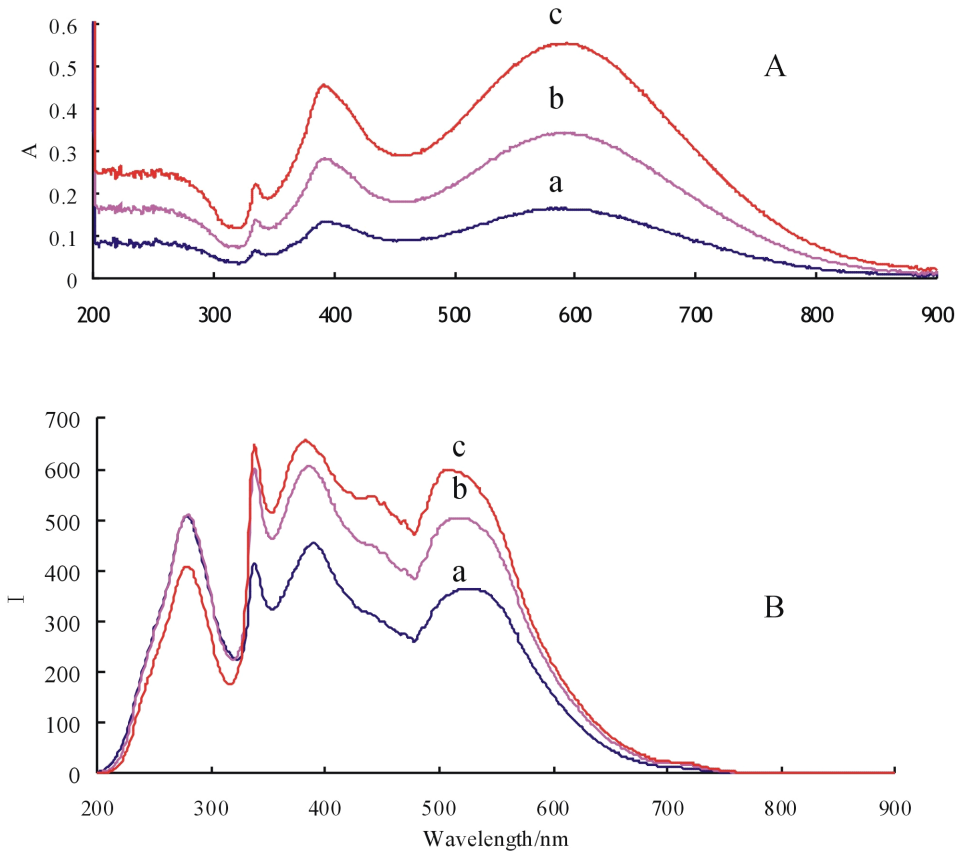

Figure 4 | **SPR spectra (A) and RRS spectra (B) of AgNPB.** (a): 2.5 × 10-5 mol/L AgNPB; (b): 5.0 × 10-5 mol/L AgNPB; (c): 7.5 × 10-5 mol/L AgNPB.

285 nm (Fig. 6S,7S). The absorbance increased slowly with the $AgNO_3$ concentration increased in the range of 12.5-100 $\times$ 10^{-6} mol/L because AgCl particles have weak absorption. In the medium of 5.0 $\times$ 10^{-4} mol/L NaCl, AgNPB has two SPR absorption peaks at 330 nm and 530 nm (Fig. 8S). The absorbance at 530 nm decreased linearly with the H_2O_2 concentration increased in the range of 2–8 $\times$ 10^{-5} mol/L H_2O_2 that can be used to determine H_2O_2.

SERS spectra of AgNP-NaCl-H_2O_2 system. SERS technology is very sensitive for the detection of nano-aggregate, and it is very important to choice a suitable molecular probe. Reportedly cationic dye rhodamine 6G was used as a sensitive SERS probe[52], but it can interact with AgNP to form aggregate and cannot be used in the analysis of AgNP-NaCl system. Victoria blue B (VBB), used as a SERS probe, had very weak Raman signals in the two systems of 9.25 $\times$ 10^{-5} mol/L AgNP and 9.25 $\times$ 10^{-5} mol/L AgNP-2.0 $\times$ 10^{-3} mol/L NaCl. With addition of H_2O_2, SERS signals enhanced due to the formation of AgCl and Ag/AgCl aggregate and the system exhibited Raman peaks at 224 cm^{-1}, 307 cm^{-1}, 351 cm^{-1}, 564 cm^{-1}, 608 cm^{-1}, 772 cm^{-1}, 1127 cm^{-1}, 1179 cm^{-1}, 1309 cm^{-1}, 1359 cm^{-1}, 1508 cm^{-1}, 1571 cm^{-1}, 1647 cm^{-1} (Fig. 9S). This demonstrated that there are AgNP/AgCl aggregates in the system.

Discussion

Mechanism of autocatalytic oxidization of AgNP. Stabile AgNP in size of 10 nm was prepared conveniently by $NaBH_4$ reduction of Ag^+. When NaCl was added, Cl^- can be adsorbed on the surface of AgNP, and the signals of SPR absorption and RRS are still very weak that indicated no aggregation in the system. After adding H_2O_2, small AgNP can catalyze H_2O_2 to produce free radicals HO· with strong oxidation ability, which can oxidize Ag atoms on the surface of AgNP to produce $[Ag^+]$ that is different with the Ag^+ from $AgNO_3$. The $[Ag^+]$ combined with Cl^- to form [AgCl] molecules which had strong hydrophobic property and then lead to form large AgNP/AgCl aggregates that enhanced the scattering signal. Small size HO· can penetrate the gap of [AgCl] molecules to further oxidize Ag atoms on inner layer of AgNP (Fig. 3), and made AgNP become smaller and its SPR absorption weaker. When H_2O_2 increased, the RRS intensity increased linearly due to more big AgNP/AgCl aggregates forming, and the SPR absorption decreased linearly due to much less small nanosilver forming. Thus, two new SPR absorption and RRS methods were established to determine H_2O_2.

According to the generation mechanism of HO· and the autocatalytic oxidation mechanism of AgNP[53,54] (AgNP = Ag_n = Ag_{m+2k}), the main reactions of AgNP-NaCl-H_2O_2 system are as follows,

$$Ag_n + H_2O_2 = Ag_n/HOOH \quad (1)$$

$$Ag_n/HOOH = Ag/HOO\cdot \quad (2)$$

$$2Ag_n/HOO\cdot = 2Ag_n + 2HO\cdot + O_2 \quad (3)$$

$$Ag_n + HO\cdot = Ag_{n-1}/[Ag^+] + H_2O \quad (4)$$

$$Ag_{n-1}/Ag^+ + Cl^- = Ag_{n-1}/AgCl \quad (5)$$

In the presence of NaCl, the reducing ability of Ag was enhanced and made the reaction of H_2O_2 oxidize AgNP to form $Ag_{m\text{-}2k}/[AgCl]_{2k}$ complex particles become easily, as the result of the formation of AgCl particle with low solubility. The total reaction is as follow,

$$Ag_{m+2k} + kH_2O_2 + 2kOH^- + 2kCl^- = 2kH_2O + kO_2 + Ag_{n-2k}/(AgCl)_{2k} \quad (6)$$

Relationship between the SPR absorption peaks and the RRS peaks of AgNPB. AgNPBs exhibited special optical property that have one sharp out-of-plane quadrupole SPR absorption peak at 330 nm (Fig. 4A), one out-of-plane dipole peak at 390 nm, and one broad in-plane dipole peak at 580 nm[54,55]. The absorbance of the three peaks was linearly increased with AgNPB concentration increased. The study of RRS spectra of nanoparticles in liquid phase shown that, their RRS peaks are closely related with the emission intensity of light source and the SPR absorption peaks[56,57]. The light source of model F-7000 Hitachi fluorescence spectrometer has the strongest emission wavelength at 280 nm that cause a scattering peak at 280 nm, and the emission intensity weaken as the increase of the wavelength. AgNPB has a sharp scattering peak at 330 nm which is corresponding to the out-of-plane quadrupole SPR absorption peak (Fig. 4B) that was called as out-of-plane quadrupole RRS peak. AgNPB has a strong RRS peak at 390 nm that was ascribed to out-of-plane dipole SPR absorption, was called as out-of-plane dipole RRS peak. Besides, the in-plane dipole peak at 530 nm is violet-shift 50 nm compare to its SPR absorption peak because the light source has strong emission at 530 nm. Though the RRS intensity of the three peaks increased with AgNPB concentration increased, they had no linear relationship since the sols exist in multiple scattering.

Analytical features. Under the selected conditions (Fig. 10S–19S), the RRS intensity at 330 nm (I) of different H_2O_2 concentration was recorded, and the working curve between ΔI and H_2O_2 concentration was drawn. The linear range of AgNP-NaCl system was 2.0 $\times$ 10^{-8}-8.0 $\times$ 10^{-5} mol/L, with a regression equation of ΔI = 71.4c-1.6, a correlation coefficient of 0.9852, and a detection limit of 8 $\times$ 10^{-9} mol/L. A 5.0 $\times$ 10^{-7} mol/L, 5.0 $\times$ 10^{-6} mol/L and 20 $\times$ 10^{-6} mol/L H_2O_2 were determined five times, and the related standard deviations (RSD) were 4.1%, 3.7% and 3.8% respectively, this showed that the RRS method has good accuracy. The linear range of AgNP-NaCl-H_2SO_4-$FeSO_4$ system was 1.0 $\times$ 10^{-7}-2.5 $\times$ 10^{-5} mol/L, with a detection limit of 2 $\times$ 10^{-8} mol/L. In the RRS analytical system, the AgNP-NaCl is most sensitive, simple, stabile and low blank (Table 1S), and it was chosen to detect H_2O_2 concentration. The SPR methods of the two systems also can be used to determine H_2O_2 with low-cost, though they were not as sensitive as RRS methods. According to the procedure, a standard solution containing 20 $\times$ 10^{-6} mol/L H_2O_2 and various coexistent compounds were examined, with a relative error of less than $\pm$ 10%. A 100 times of ClO_4^- and SO_4^{2-}, 70 times of Ca(II) and Mg(II), 50 times of Cu^{2+}, Mo^{6+}, I^-, triethanolamine, Co^{2+}, NO_2^-, 10 times of Mn^{2+}, Br^-, citric acid, and 2.5 mg/L HSA did not interfere with the determination. This indicated that the method has good selectivity.

Methods

Apparatus and reagents. A Model F-7000 fluorescence spectrophotometer (Hitachi Company, Japan) was used to record the RRS spectra by means of synchronous scanning excitation wavelength λ_{ex} and emission wavelength λ_{em} (λ_{ex}-λ_{em} = $\Delta\lambda$ = 0) and the RRS intensity. A Model TU-1901 double beams spectrophotometer (Puxi Tongyong Apparatus Limited Company, Beijing) was used to record the SPR spectra and the SPR intensity. A model JSM-6380LV scanning electron microscope (Electronic Stock Limited Company, Japan), a model of JEM-2100F field emission transmission electron microscope (Electronic Stock Limited Company, Japan), a model DXR smart Raman spectrometer (Thermo Fisher Scientific Co., Ltd., USA), a moldel SK8200LH ultrasonic reactor (Kedao Company, Shanghai, China), and a model magnetic stirrer (Zhongda Instrumental Plant, Jiangsu, China) were used.

A 1.0 $\times$ 10^{-3} mol/L $AgNO_3$ solution, 1% (W/V) sodium citrate solution, 0.05 mol/L NaCl solution, and 1.0 $\times$ 10^{-3} mol/L $FeSO_4$ solution were used. A 0.05% (W/V) $NaBH_4$ was prepared freshly. A 0.100 mol/L H_2O_2 standard solution was prepared as follows: 1.02 mL H_2O_2 (30%) was diluted to 100 mL with water, it was standardized by KMnO4 procedure, and was diluted to 5.00 $\times$ 10^{-4} mol/L before use.

A 1.85 $\times$ 10^{-4} mol/L AgNP was prepared as follows: 9.25 mL 1.0 $\times$ 10^{-3} mol/L $AgNO_3$ and 3.5 mL 1% trisodium citrate were added into a conical flask with stirring and diluted to 40 mL with water, then 4 mL 0.05% $NaBH_4$ was added slowly with about 15 min, the mixture was diluted to 50 mL, and it can be used after 24 h to make the $NaBH_4$ decomposing completely. The preparation of AgNP sols was repeated five times, the SPR peak is at 395 nm with an average absorption value of 2.50 $\pm$ 0.10, and the sols were stabile within 20 days (Fig.20S). A 1.0 $\times$ 10^{-4} mol/L AgNPB was prepared as follows: 40 mL of water, 500 μL 1.0 $\times$ 10^{-2} mol/L $AgNO_3$, 1.5 mL 6.0 $\times$ 10^{-2} mol/L sodium citrate, 120 μL 30% H_2O_2, and 200 μL 0.1 mol/L $NaBH_4$ were added into a triangle flask in turn with constantly stirring for 15 min. Then heat to

boil for 5 min to get rid of the excess H_2O_2 and the solution was diluted to 50 mL. All reagents were of analytical grade and the water was highly pure sub-boiling water.

Procedure. A 1.0 mL 1.85×10^{-4} mol/L AgNP solution, 80 μL 0.05 mol/L NaCl (or adding 80 μL 5.0×10^{-2} mol/L H_2SO_4, 75 μL 1.0×10^{-3} mol/L $FeSO_4$), and a certain amount of H_2O_2 solution were added into a 5 mL calibrated tube in turn, then diluted to 2 mL and mixed well. The RRS intensity at 330 nm (I) was recorded by a fluorescence spectrophotometer with synchronous scanning (λ_{ex}-$\lambda_{em} = \Delta\lambda = 0$). A blank ($I_0$) without H_2O_2 was recorded and the value of $\Delta I = I–I_0$ was calculated.

1. Ke, J. *et al.* Dopant-induced modification of active site structure and surface bonding mode for high-performance nanocatalysts: CO oxidation on capping-free (110)-oriented CeO_2:Ln (Ln = La-Lu) nanowires. *J. Am. Chem. Soc.* **135**, 15191–15200 (2013).
2. Zhang, S. *et al.* In-situ studies of nanocatalysis. *Acc. Chem. Res.* **46**, 1731–1739 (2013).
3. Dutta, S. *et al.* Silver nanoparticle decorated reduced graphene oxide (rGO) nanosheet: a platform for SERS based low-level detection of uranyl ion. *ACS Appl. Mater. Interfaces* **5**, 8724–8732 (2013).
4. Veerakumar, P., Ramdass, A. & Rajagopal, S. Ruthenium nanocatalysis on redox reactions. *J. Nanosci. Nanotechnol.* **13**, 4761–4786 (2013).
5. Borys, N. J., Shafran, E. & Lupton, J. M. Surface plasmon delocalization in silver nanoparticle aggregates revealed by subdiffraction supercontinuum hot spots. *Sci. Rep.* **3**, 2090 (2013).
6. Chen, P. *et al.* Single-molecule fluorescence imaging of nanocatalytic processes. *Chem. Soc. Rev.* **39**, 4560–4570 (2010).
7. Wen, G. Q., Liang, A. H. & Jiang, Z. L. Functional nucleic acid nanoparticle-based resonance scattering spectral probe. *Plasmonics* **8**, 899–911 (2013).
8. Zhu, Z. *et al.* Manipulation of collective optical activity in one-dimensional plasmonic assembly. *ACS Nano* **6**, 2326–2332 (2012).
9. Negreiros, F. R. *et al.* A first-principles theoretical approach to heterogeneous nanocatalysis. *Nanoscale* **4**, 1208–1219 (2012).
10. Fihri, A. *et al.* Nanocatalysts for Suzuki cross-coupling reactions. *Chem. Soc. Rev.* **40**, 5181–5203 (2011).
11. Chng, L. L., Erathodiyil, N. & Ying, J. Y. Nanostructured catalysts for organic transformations. *Acc. Chem. Res.* **46**, 1825–1837 (2013).
12. Roldan, C. B. Metal nanoparticle catalysts beginning to shape-up. *Acc. Chem. Res.* **46**, 1682–1691 (2013).
13. Li, L. *et al.* Selective synthesis of Cu_2O nanocrystals as shape-dependent catalysts for oxidative arylation of phenylacetylene. *Chemistry* **18**, 10491–6 (2012).
14. Kalidindi, S. B. & Jagirdar, B. R. Nanocatalysis and prospects of green chemistry. *ChemSusChem.* **5**, 65–75 (2012).
15. Yao, D. M., Wen, G. Q. & Jiang, Z. L. A highly sensitive and selective resonance Rayleigh scattering method for bisphenol A based on the aptamer-nanogold catalysis of $HAuCl_4$-vitamine C particle reaction. *RSC Adv.* **3**, 13353–13356 (2013).
16. Cao, C. *et al.* Dual enlargement of gold nanoparticles: from mechanism to scanometric detection of pathogenic bacteria. *Small* **7**, 1701–1708 (2011).
17. Mohamed, M. B. *et al.* Growth mechanism of anisotropic gold nanocrystals via microwave synthesis: formation of dioleamide by gold nanocatalysis. *ACS Nano* **4**, 2766–72 (2010).
18. Harding, C. *et al.* Control and manipulation of gold nanocatalysis: effects of metal oxide support thickness and composition. *J. Am. Chem. Soc.* **131**, 538–548 (2009).
19. Yang, P. & Huo, R. T. Influence of Coupling Agents modification on photocatalysis activity of nano-TiO_2. *J. Chin. Ceram. Soc.* **41**, 409–415 (2013).
20. Jiang, Z. L. *et al.* Resonance scattering assay for trace human chorionic gonadotrophin using gold-platinum nanoalloy immunoprobe as catalyst. *Acta Chim. Sin.* **70**, 1748–1754 (2012).
21. Wen, G. Q., Liang, A. H. & Jiang, Z. L. Functional nucleic acid nanoparticle-based resonance scattering spectral probe. *Plasmonics* **8**, 899–911 (2013).
22. Kung, C. C. *et al.* Preparation and characterization of three dimensional graphene foam supported platinum-ruthenium bimetallic nanocatalysts for hydrogen peroxide based electrochemical biosensors. *Biosens. Bioelectron.* **52**, 1–7 (2014).
23. Tang, J. *et al.* In situ amplified electronic signal for determination of low-abundance proteins coupling with nanocatalyst-based redox cycling. *Chem. Commun.* **49**, 1530–1532 (2013).
24. Jiang, Z. L., Qin, H. M. & Liang, A. H. A new nanocatalytic spectrophotometric assay for cationic surfactant using phosphomolybdic acid-formic acid-nanogold as indicator reaction. *Chin. J. Chem.* **30**, 59–64 (2012).
25. Dong, J. C., Liang, A. H. & Jiang, Z. L. A highly sensitive resonance Rayleigh scattering method for hemin based on the aptamer-nanogold probe catalysis of citrate-$HAuCl_4$ particle reaction. *RSC Adv.* **3**, 17703–17706 (2013).
26. Lai, W. Z. *et al.* Preparation and optical properties of triangular silver nanoplates by a dual reduction method. *Acta Phys. Chim. Sin.* **26**, 1177–1183 (2010).
27. Jin, R. C., Cao, Y. W. & Mirkin, C. A. Photoinduced conversion of silver nanospheres to nanoprisms. *Science* **294**, 1901–1903 (2001).
28. Jiang, Z. L., Zhou, L. P. & Liang, A. H. Resonance scattering detection of trace melamine using aptamer-modified nanosilver probe as catalyst without separation of its aggregations. *Chem. Comm.* **47**, 3162–3164 (2011).
29. Cooper, W. J., Zika, R. G. & Petasne, R. G. Photochemical formation of hydrogen peroxide in natural waters exposed to sunlight. *Environ. Sci. Technol.* **22**, 1156–1160 (1988).
30. Rica, R. & Stevens, M. M. Plasmonic ELISA for the ultrasensitive detection of disease biomarkers with the naked eye. *Nat. Nanotechnol.* **7**, 821–824 (2012).
31. Slimane, M. *et al.* Influence of experimental parameters on sonochemistry dosimetries: KI oxidation, Fricke reaction and H_2O_2 production. *J. Haz. Mat.* **178**, 1007–1014 (2010).
32. Wang, Z. H. *et al.* Graphene-amplified electrogenerated chemiluminescence of CdTe quantum dots for H_2O_2 sensing. *Luminescence* **28**, 259–264 (2013).
33. Abbas, M. E. *et al.* Fluorometric determination of hydrogen peroxide in milk by using a Fenton reaction system. *Food Chem.* **120**, 327–331 (2010).
34. Chai, X. S. *et al.* Rapid determination of hydrogen peroxide in the wood pulp bleaching streams by a dual-wavelength spectroscopic method. *Anal. Chim. Acta* **507**, 281–284 (2004).
35. Luo, W. *et al.* Rapid quantitative determination of hydrogen peroxide by oxidation decolorization of methyl orange using a Fenton reaction system. *Anal. Chim. Acta* **629**, 1–6 (2008).
36. Dreaden, E. C. *et al.* The golden age: gold nanoparticles for biomedicine. *Chem. Soc. Rev.* **41**, 2740–2779 (2012).
37. Song, Y. J., Wei, W. L. & Qu, X. G. Colorimetric Biosensing Using Smart Materials. *Adv. Mater.* **23**, 4215–4236 (2011).
38. Liu, X. *et al.* A one-step homogeneous immunoassay for cancer biomarker detection using gold nanoparticle probes coupled with dynamic light scattering. *J. Am. Chem. Soc.* **130**, 2780–2278 (2008).
39. Guo, Y. M. *et al.* Colorimetric detection of mercury, lead and copper ions simultaneously using protein-functionalized gold nanoparticles. *Biosen. Bioelectron.* **26**, 4064–4069 (2011).
40. Liu, J. M. *et al.* Ultra-sensitive non-aggregation colorimetric sensor for detection of iron based on the signal amplification effect of Fe^{3+} catalyzing H_2O_2 oxidize gold nanorods. *Talanta* **116**, 199–204 (2013).
41. Tripathy, S. K., Woo, J. Y. & Han, C. S. Highly selective colorimetric detection of hydrochloric acid using unlabeled gold nanoparticles and an oxidizing agent. *Anal. Chem.* **83**, 9206–9212 (2011).
42. Diez, I. & Ras, R. H. A. Fluorescent silver nanoclusters. *Nanoscale* **3**, 1963–1970 (2011).
43. Zhang, M. & Ye, B. C. Colorimetric chiral recognition of enantiomers using the nucleotide-capped silver nanoparticles. *Anal. Chem.* **83**, 1504–1509 (2011).
44. Thompson, D. G. *et al.* Ultrasensitive DNA detection using oligonucleotide silver nanoparticle conjugates. *Anal. Chem.* **80**, 2805–2810 (2008).
45. Li, K. *et al.* A stable and reproducible nanosilver-aggregation-4-mercaptopyridine surface-enhanced Raman scattering probe for rapid determination of trace Hg^{2+}. *Talanta* **99**, 890–896 (2012).
46. Liu, Y. & Huang, C. Z. Screening sensitive nanosensors via the investigation on shape-dependent localized surface plasmon resonance of single Ag nanoparticles. *Nanoscale* **5**, 7458–7466 (2013).
47. Wu, Y. G. *et al.* Nanoparticles assembled by aptamers and crystal violet for arsenic(III) detection in aqueous solution based on a resonance Rayleigh scattering spectral assay. *Nanoscale* **4**, 6841–6849 (2012).
48. Fu, X. B. *et al.* A label-free thrombin binding aptamer as a probe for highly sensitive and selective detection of lead(II) ions by a resonance Rayleigh scattering method. *Analyst* **137**, 1097–1099 (2012).
49. Mie, G. Beitrage zur optik trüber medien, speziel kolloidaler metallosungen. *Ann. Phys.* **25**, 377–445 (1908).
50. Sun, Y. G., Gates, B. & Mayers, B. Crystalline silver nanowires by soft solution processing. *Nano Lett.* **2**, 165–168 (2002).
51. Jain, P. K., Eustis, S. & El-Sayed, M. A. Plasmon coupling in nanorod assemblies: optical absorption, discrete dipole approximation simulation, and exciton-coupling model. *J. Phys. Chem. B* **110**, 18243–8253 (2006).
52. Jiang, Z. L. *et al.* A label-free nanogold DNAzyme-cleaved surface-enhanced resonance Raman scattering method for trace UO_2^{2+} using rhodamine 6G as probe. *Plasmonics* **8**, 803–810 (2013).
53. Novikov, A. S. *et al.* Generation of HO· radical from hydrogen peroxide catalyzed by aqua complexes of the group III metals $[M(H_2O)_n]^{3+}$ (M = Ga, In, Sc, Y, or La): A theoretical study. *ACS Catal.* **3**, 1195–1208 (2013).
54. Maillard, M., Huang, P. & Brus, L. Ag nanodisk growth by surface plasmon enhanced photoreduction of adsorbed $[Ag^+]$. *Nano Lett.* **3**, 1611–1615 (2003).
55. Jiang, P., Li, S. Y. & Xie, S. S. Machinable long PVP-stabilized silver nanowires. *Chem. Eur. J.* **10**, 4817–4821 (2004).
56. Liang, A. H. *et al.* Surface plasmon resonance effect of nanogold/silver and its analytical application. *Tr. Anal. Chem.* **37**, 32–47 (2012).
57. Jiang, Z. L. *et al.* Nanocatalytic resonance scattering spectral analysis. *Sci. China Chem.* **53**, 1049–1054 (2010).

Acknowledgments

This work supported by the National Natural Science Foundation of China (No. 21267004, 21307017, 21367005, 21365011), the Research Funds of Guangxi Key Laboratory of Environmental Pollution Control Theory and Technology, the Natural Science Foundation of Guangxi (No. 2013GXNSFFA019003, 2013GXNSFAA019046), and the Research Funds of Guangxi Education Department (No. 2013YB234, 2013YB035).

Author contributions

G.Q.W. and Y.H.L. performed the experiment and measurement analysis. G.Q.W. and Z.L.J. prepared Fig.1–4. A.H.L. and Z.L.J. contributed to the discussion and measurement analysis. All authors contributed to the preparation of the manuscript and reviewed the manuscript.

Additional information

Supplementary information accompanies this paper at http://www.nature.com/scientificreports

Competing financial interests: The authors declare no competing financial interests.

How to cite this article: Wen, G.Q., Luo, Y.H., Liang, A.H. & Jiang, Z.L. Autocatalytic Oxidization of Nanosilver and Its Application to Spectral Analysis. *Sci. Rep.* **4**, 3990; DOI:10.1038/srep03990 (2014).